Robust μ-Synthesis Control of Dual LCL Type IPT System Considering Load and Mutual Inductance Uncertainty

CHENYANG XIA [1], (Member IEEE), **QIQI SUN**[1], **XINYU LI**[1], **AND AIGUO PATRICK HU**[2]

[1]School of Electrical and Power Engineering, China University of Mining and Technology, Xuzhou 221116, China
[2]Department of Electrical and Computer Engineering, The University of Auckland, Auckland 1010, New Zealand

Corresponding author: Chenyang Xia (18260722082@163.com)

ABSTRACT The output voltage of a dual LCL inductive power transfer (IPT) system varies with the load and mutual inductance, which can affect the system performance, e.g., the charging speed of electrical equipment. This paper proposes a robust controller to maintain constant output voltage against the load and mutual inductance variations. A μ-synthesis method is proposed based on structured singular value to design the dual LCL IPT closed-loop system. The frequency-domain nominal model of the system is established by using the generalized state-space averaging (GSSA) method. A standard M-Δ configuration is generalized through separating the nominal and uncertain block by upper linear fractional transformation (LFT). The μ-controller is finally obtained by D–K iteration. The robust performance analysis and time-domain performance analysis are also carried out. The simulation and experimental results verified the effectiveness of the proposed modeling and controller design, and demonstrated the robust stability and robust performance of the dual LCL IPT system.

INDEX TERMS Generalized state-space averaging (GSSA), inductive power transfer (IPT), robust control, μ-synthesis.

I. INTRODUCTION

Inductive power transfer (IPT) based on electromagnetic induction is a popular wireless power transfer technology, which has attracted the attention of scholars and researchers in recent years. It has been widely adopted in electric vehicles [1]–[2], rail transit [3]–[4], household appliances [5], implantable medical devices [6], wearable mobile devices [7], etc.

For an IPT system, variation of circuit parameters, such as load and mutual inductance, are a common phenomenon due to specific operating conditions of the system, which will cause random drift of inherent resonant frequency of the resonant circuit [8], the reduction of the power transmission capacity and system performances to a certain extent, and

The associate editor coordinating the review of this manuscript and approving it for publication was Ho Ching Iu.

also affect the stable operation of the system [9]. In order to solve these aforementioned issues, more and more research methods such as circuit topology optimization and advanced control strategies are carried out. One way to reduce the effects of uncertainties is to use special circuit structures such as capacitor-inductor-capacitor (CLC) [10], inductor-capacitor-inductor (LCL) [11] or series-parallel-series (SPS) [12] compensation topologies, which can provide constant voltage or current characteristics with a single parameter change without feedback control and communication between the primary and secondary sides. Another way to deal with uncertainties is to adopt control methods. There are some single-objective control methods without system modeling including dynamic tuning method [13] and pulse density modulation self-oscillation tuning frequency tracking method [14], so as to ensure the operating frequency of the system is consistent with the resonant frequency of the

resonant network. However, the above research methods rely on the resonant compensation topologies, and the adaptability, stability as well as robustness of multi-parameter variation are slightly poor without establishing a more accurate system mathematical model. Therefore, the system behaviors (*ie*, transient and steady-state characteristics) and closed-loop control design based on system parameter modeling are widely studied.

A closed-loop digital PI controller based on an approximate small-signal model for LCL-T structure [15] and a new adaptive sliding-mode control scheme [16] were designed to achieve good reference tracking performance of the system, but these have poor robustness due to high-order and nonlinear characteristics of the system. Besides, there exists difficult to eliminate the negative effects of external interference and parameters variation. *Li*, et al proposed a two-degree-of-freedom H_∞ controller for SS-IPT system which can effectively improve the transient performance on the basis of guaranteeing the robustness of the voltage stabilization [17]. A closed-loop system of the relay structure which is applied in an EV charging system considering load uncertainty and external disturbance has achieved good tracking of the reference output voltage and robustness [18]. H_∞ optimal approach for CLC-type system considering frequency variation can achieve robust stability against unstructured uncertainties and nominal performance requirement, but it neglects robust performance requirement [19]. Due to the comprehensive consideration of the above factors, structured singular value μ analysis method has been proposed to test the robust stability and robust performance (RSRP) of a system considering structured perturbations, which can avoid the conservatism of H_∞ control design [29]–[32]. In view of the frequency uncertainties of CLC-type structure [20] and the coupling coefficient variation in the case of different position offsets based on SP-type structure [21], μ-synthesis control system is designed to realize RSRP, which is verified to achieve good performance and is applicable to other structures.

Although robust control has been widely used in an IPT system, it can be found that the current research mainly focuses on single parameter variation. Multi-parameter variation is a common phenomenon in IPT systems while due to the complexity of the system structure. Therefore, taking into account the control requirements of multi-parameter variation of the system and the applicability of μ control in non-conservativeness aspects, this paper proposes a robust μ-controller considering the perturbation of load and mutual inductance to achieve effective control output of the closed-loop system. This study takes an LCL resonant topology as an example, which generates strong resonance and a high power factor for reducing voltage and current stresses on the primary power converter [22]. This topology is also widely used in energy bidirectionally fed power transmission systems.

The rest of this paper is arranged as follows: Section II briefly introduces the working principle of dual LCL IPT
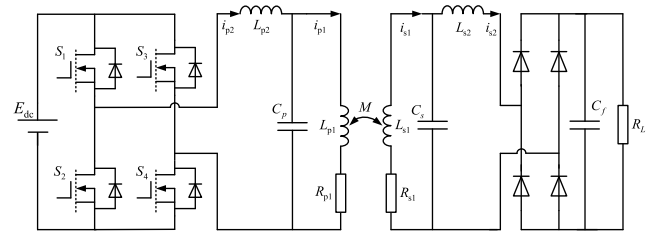

FIGURE 1. Dual LCL type IPT system circuit topology.

system. In Section III, the frequency-domain linear model and the uncertainties model of load and mutual inductance parameter perturbation adopted linear fractional transformation (LFT) are built up. In Section IV, a standard M-Δ structure for robust stability is established and the robust performance is analyzed. The D-K iterative algorithm is used to design the μ-controller. Finally, the simulation and experimental results in Section V further verify the RSRP of the closed-loop system based on the μ-controller and realize good robustness.

II. WORKING PRINCIPLE OF DUAL LCL IPT SYSTEM
The circuit structure diagram of the dual LCL IPT system is shown in Fig. 1. The whole system can be divided into the primary side and the secondary side. Regarding the primary side, the DC voltage E_{dc} is the system input, which is obtained by the AC voltage through rectification, voltage regulation and filtering. The high-frequency inverter network is composed of two switch pairs (S_1, S_4), (S_2, S_3)), which outputs high frequency AC energy to the resonant network (LCL type resonant network, consisting of L_{p1}, L_{p2} and C_p) through alternately switching. For the secondary side, it is composed of the LCL type resonant network (consisting of L_{s1}, L_{s2}, and C_s), the rectifying network (consisting of four rectifying diodes), the filtering network (consisting of C_f), and the load R_L.

For the IPT system, the resonant frequency of the resonant network and the switching frequency of the inverter are kept consistent to ensure the power factor of the resonant network is 1, and the natural resonant frequency ω_0 is expressed as:

$$\omega_0 = \frac{1}{\sqrt{L_{p2}C_p}} = \frac{1}{\sqrt{L_{p1}C_p}} \tag{1}$$

The root mean square (RMS) value of the output voltage U_{in} of the inverter can be expressed as

$$U_{in} = \frac{2\sqrt{2}}{\pi}E_{dc} \tag{2}$$

When the whole network is in resonance state, the resonance network parameters satisfy the following condition according to the design requirements of the system.

$$\begin{cases} X_{L_{p1}} = X_{L_{p2}} \\ X_{L_{s2}} = X_{L_{s1}} \end{cases} \tag{3}$$

According to the principle of electromagnetic induction, the value of the secondary side induced voltage U_{oc} is expressed as (4), where M represents the mutual inductance between the primary and secondary side coils.

$$U_{oc} = \omega_0 M I_{p1} \qquad (4)$$

Based on the principle of power conservation, R_{eq} is the equivalent input resistance of the rectifier given as (5), where U_{oc} is RMS of the secondary side open circuit voltage, U_o is the load output voltage and Q_s is quality factor [23].

$$R_{eq} = \frac{U_{oc}^2 Q_s^2 R_L}{U_o^2} \qquad (5)$$

III. MODELING OF DUAL LCL IPT SYSTEM
In order to study the dynamic behavior characteristics of the system under parameters perturbation, it is necessary to establish the mathematical model of system for analysis.

A. GENERALIZED STATE SPACE AVERAGING MODEL
The inductor currents and capacitor voltages in the circuit are selected as state variables, so the state variables of the dual LCL-type IPT system is $x(t) = [i_{p2}, u_{Cp}, i_{p1}, i_{s1}, u_{Cs}, i_{s2}, U_{Cf}]^T$, and the zero-order harmonic component is used to represent the DC component such as U_{Cf}. The even harmonic component of the state variables $i_{p2}, u_{Cp}, i_{p1}, i_{s1}, u_{Cs}, i_{s2}$ with AC characteristics are approximately zero. The odd harmonic component represents AC characteristic components. Each state variable exhibits better sinusoidal characteristics when the LCL network operates at resonance conditions. Therefore, the fundamental component can be used to approximate these time-domain state variables, which are defined as:

$$
\begin{cases}
i_{p2} = \langle i_{p2}\rangle_1 e^{j\omega_0 t} + \langle i_{p2}\rangle_{-1} e^{-j\omega_0 t} \\
u_{Cp} = \langle u_{Cp}\rangle_1 e^{j\omega_0 t} + \langle u_{Cp}\rangle_{-1} e^{-j\omega_0 t} \\
i_{p1} = \langle i_{p1}\rangle_1 e^{j\omega_0 t} + \langle i_{p1}\rangle_{-1} e^{-j\omega_0 t} \\
i_{s1} = \langle i_{s1}\rangle_1 e^{j\omega_0 t} + \langle i_{s1}\rangle_{-1} e^{-j\omega_0 t} \\
u_{Cs} = \langle u_{Cs}\rangle_1 e^{j\omega_0 t} + \langle u_{Cs}\rangle_{-1} e^{-j\omega_0 t} \\
i_{s2} = \langle i_{s2}\rangle_1 e^{j\omega_0 t} + \langle i_{s2}\rangle_{-1} e^{-j\omega_0 t} \\
U_{Cf} = \langle U_{Cf}\rangle_0
\end{cases} \qquad (6)
$$

where $\langle\cdot\rangle_0$ and $\langle\cdot\rangle_1$ (or $\langle\cdot\rangle_{-1}$) respectively denote the zero-order and first-order Fourier coefficients of the circuit variables. Furthermore, $\langle\cdot\rangle_{-1}$ represents the complex conjugation of $\langle\cdot\rangle_1$.

The state variables of the GSSA model is set as follows:

$$x(t) = [\langle i_{p2}\rangle_1, \langle u_{Cp}\rangle_1, \langle i_{p1}\rangle_1, \langle i_{s1}\rangle_1, \langle u_{Cs}\rangle_1, \langle i_{s2}\rangle_1, \langle U_{Cf}\rangle_0]^T \qquad (7)$$

According to the circuit topology of the system, with the GSSA modeling method [24], the generalized differential equations are established as follows:

$$
\begin{cases}
\dfrac{d\langle i_{p2}\rangle_1}{dt} = -\dfrac{1}{L_{p2}}\langle V_{cp}\rangle_1 + \dfrac{1}{L_{p2}}\langle E_{dc}s(t)\rangle_1 - j\omega\langle i_{p2}\rangle_1 \\[2mm]
\dfrac{d\langle u_{Cp}\rangle_1}{dt} = \dfrac{1}{C_p}\langle i_{p2}\rangle_1 + \dfrac{1}{C_p}\langle i_{p1}\rangle_1 - j\omega\langle u_{Cp}\rangle_1 \\[2mm]
\dfrac{d\langle i_{p1}\rangle_1}{dt} = \dfrac{-L_{s1}}{\Delta}\langle u_{Cp}\rangle_1 - \dfrac{L_{s1}R_{p1}}{\Delta}\langle i_{p1}\rangle_1 \\[1mm]
\qquad + \dfrac{M}{\Delta}\langle u_{Cs}\rangle_1 + \dfrac{MR_{s1}}{\Delta}\langle i_{s1}\rangle_1 - j\omega\langle i_{p1}\rangle_1 \\[2mm]
\dfrac{d\langle i_{s1}\rangle_1}{dt} = \dfrac{-M}{\Delta}\langle u_{Cp}\rangle_1 - \dfrac{MR_{p1}}{\Delta}\langle i_{p1}\rangle_1 \\[1mm]
\qquad + \dfrac{L_{p1}}{\Delta}\langle V_{cs}\rangle_1 + \dfrac{L_{p1}R_{s1}}{\Delta}\langle i_{s1}\rangle_1 - j\omega\langle i_{s1}\rangle_1 \\[2mm]
\dfrac{d\langle u_{Cs}\rangle_1}{dt} = \dfrac{1}{C_s}\langle i_{s1}\rangle_1 + \dfrac{1}{C_s}\langle i_{s2}\rangle_2 - j\omega\langle u_{Cs}\rangle_1 \\[2mm]
\dfrac{d\langle i_{s2}\rangle_1}{dt} = -\dfrac{1}{L_{s2}}\langle u_{Cs}\rangle_1 + \dfrac{1}{L_{s2}}\langle u_{Cs}sgn(t)\rangle_1 - j\omega\langle i_{s2}\rangle_1 \\[2mm]
\dfrac{d\langle U_{Cf}\rangle_0}{dt} = \dfrac{1}{C_f}\langle i_{s2}sgn(t)\rangle_0 - \dfrac{1}{C_f R_f}\langle U_{Cf}\rangle_0
\end{cases} \qquad (8)
$$

where $\Delta = L_{p1}*L_{s1}-M*M$; $s(t)$ represents the primary side inverter link switching function, and sgn(t) is the switching function of the secondary side rectification link, which are expanded by Fourier series. By circuit analysis, the phase difference is $\pi/2$, that is $\theta = \pi/2$.

$$\langle s(t)\rangle_1 = \frac{-2j}{\pi} \qquad (9)$$

$$\langle sgn(t)\rangle_k = \begin{cases} \dfrac{-2}{k\pi}(j\cos(k\theta) + \sin(k\theta), & k = 1,3,5... \\ 0, & k = 2,4,6... \end{cases} \qquad (10)$$

Decompose the selected state variables to obtain the generalized state variables of the system.

$$
\begin{aligned}
x(t) = [&Re\langle i_{p2}\rangle_1, Im\langle i_{p2}\rangle_1, Re\langle u_{Cp}\rangle_1, Im\langle u_{Cp}\rangle_1, Re\langle i_{p1}\rangle_1, \\
&Im\langle i_{p1}\rangle_1, Re\langle i_{s1}\rangle_1, Im\langle i_{s1}\rangle_1, Re\langle u_{Cs}\rangle_1, Im\langle u_{Cs}\rangle_1, \\
&Re\langle i_{s2}\rangle_1, Im\langle i_{s2}\rangle_1, Re\langle U_{Cf}\rangle_0]^T
\end{aligned} \qquad (11)
$$

The GSSA nominal model of the double LCL type system is obtained:

$$\begin{cases} \dot{x} = Ax + Bu \\ y = Cx + Du \end{cases} \qquad (12)$$

where A, C, D is a constant system matrix, and B is a constant control matrix (Appendix A), y is the output voltage U_{Cf}. Moreover, Decoupling of state variables and switching variables ($s(t)$ and sgn(t)) are realized from time domain to frequency domain. The nonlinear dual LCL-type IPT system has been successfully approximated to a linear system.

B. UNCERTAINTY MODEL UNDER PARAMETER PERTURBATION
In the dual LCL type IPT system, the uncertainty of the load R_L and the mutual inductance M is considered in the model. The ranges of variation of R_L and M directly affect

system performance. Mathematically, parameters uncertainty can be represented as (13) and (14).

$$1/R_L = 1/R_0(1 + p_R\delta_R) \tag{13}$$

$$M = M_0(1 + p_M\delta_M) \tag{14}$$

where R_0 and M_0 are the nominal design value of load and mutual inductance respectively. p_R and p_M denote the range of the parametric uncertainties, and $||\delta_R||_\infty \leq 1$ and $||\delta_M||_\infty \leq 1$ imply the boundedness of uncertainty. Considering the requirement of following practical experiment in the design of this paper, $p_R = 0.5$ represents the change in the range of $\pm 50\%$ of nominal value R_0 and $p_M = 0.3$ represents the change in the range of $\pm 30\%$ of nominal value M_0. The designed controller does not suffer from input saturation since the range of parameter variation is relatively small.

Based on the principle of LFT, the reciprocal $1/R_L$ for load can be expressed as $1/R_L = F_u(M_R, \delta_R)$ shown in Fig. 2 (a). The mutual inductance M can be expressed as $M = F_u(M_M, \delta_M)$ shown in Fig. 2 (b). M_R and M_M can be defined as the following forms:

$$M_R = \begin{bmatrix} -p_R & 1/R_0 \\ -p_R & 1/R_0 \end{bmatrix}, \quad M_M = \begin{bmatrix} 0 & M_0 \\ p_M & M_0 \end{bmatrix} \tag{15}$$
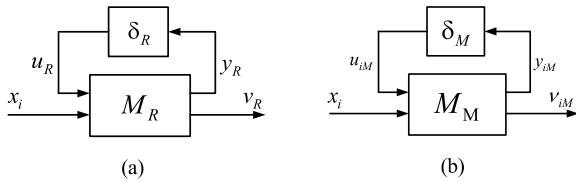

FIGURE 2. LFT of uncertain parameters (a) LFT of R_L; (b) LFT of M.

y_R and u_R are the input and output of δ_R. y_{iM} and u_{iM} are the input and output of δ_M respectively. x_i represents the state variables of the system, $v_R = x_i*1/R_L$, $v_{iM} = x_i*M$. Therefore, the relationship between the separated nominal part and the uncertain part can be expressed as:

$$\begin{bmatrix} y_R \\ v_R \end{bmatrix} = \begin{bmatrix} -p_R & 1/R_0 \\ -p_R & 1/R_0 \end{bmatrix} \begin{bmatrix} u_R \\ x_i \end{bmatrix} = \begin{bmatrix} -p_R u_R + x_i/R_0 \\ -p_R u_R + x_i/R_0 \end{bmatrix} \tag{16}$$

$$\begin{bmatrix} y_{iM} \\ v_{iM} \end{bmatrix} = \begin{bmatrix} 0 & M_0 \\ p_M & M_0 \end{bmatrix} \begin{bmatrix} u_{iM} \\ x_i \end{bmatrix} = \begin{bmatrix} M_0 x_i \\ p_M u_{iM} + M_0 x_i \end{bmatrix} \tag{17}$$

The uncertain part of the state variable constitutes the system's uncertainty matrix Δ expressed as (18) and the norm condition $||\Delta||_\infty < 1$ is satisfied. The definition of y_p and u_p are the input and the output of Δ respectively.

$$\Delta = diag\{\delta_M, \delta_R\} \tag{18}$$

$$\begin{cases} y_P = pertin = [y_{3M}, y_{4M}, ..., y_{10M}, y_R]^T \\ u_P = pertin = [u_{3M}, u_{4M}, ..., u_{10M}, u_R]^T \end{cases} \tag{19}$$

Therefore, the uncertainty model of the system can be transformed into linear dynamic system with perturbation feedback:

$$\begin{cases} \dot{x} = Ax + B_1 u_p + B_2 u \\ y_p = C_1 x + D_{11} u_p + D_{12} u \\ y = C_2 x + D_{21} u_p + D_{22} u \end{cases} \tag{20}$$

$$G = \begin{bmatrix} A & B_1 & B_2 \\ C_1 & D_{11} & D_{12} \\ C_2 & D_{21} & D_{22} \end{bmatrix} \tag{21}$$

Equation (19), $x \in R^{13}$ is the generalized state variable; u is input voltage signal E_{dc}; y is the load output voltage; Thus, a generalized controlled object G can be obtained as (21) (in Appendix B).

IV. CLOSED LOOP CONTROL SYSTEM DESIGN AND PERFORMANCE ANALYSIS

The controller design of the closed-loop system will be carried out based on the above established generalized space model and system performance requirements will also be verified in this subsection.

A. μ-CONTROLLER DESIGN

In the dual LCL IPT system, a robust feedback μ-controller $u(s)= K(s)y(s)$ is designed based on the diagram of Fig. 3.
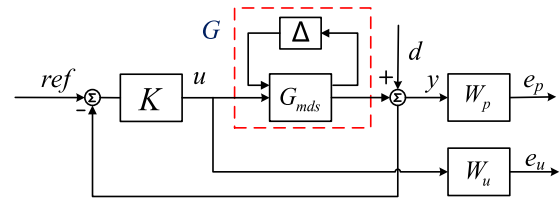

FIGURE 3. Feedback control diagram based on μ-controller.

In Fig. 3, the output voltage reference value is represented by *ref*; d is the external interference; u is the controller output, y is the system output; K is the μ-controller;

G(s) is the transfer function of the controlled object with parameter perturbation which is $G = F_u(G_{mds}, \Delta)$. the sensitivity function S is defined to represent the transfer function of the closed-loop system from reference input *ref* to error signal e when disturbance d is 0, or the transfer function from disturbance d to output y when reference input *ref* is 0, that is:

$$S(s) = [I + G(s)K(s)]^{-1} \tag{22}$$

W_p is a weighting function of the sensitivity function S. W_p is a low-pass filter with the same bandwidth as the disturbance, which is used to describe the spectrum characteristics of the disturbance and has low-pass properties. The gain of S is minimized so as to suppress disturbance with regularly occurring in the low frequency region. Therefore, the weighting function in the low frequency band should be as large as possible. Under the premise of satisfying the dynamic quality requirements of the system without increasing the order of the controller, it can be selected as follows:

$$W_p(s) = \frac{k_p}{j\omega/\omega_p + 1} \tag{23}$$

where $\omega_p = \omega_c \geq \omega_L$, the expected open-loop cut-off frequency of the system is ω_c. The bandwidth of low frequency disturbance is ω_L so that the closed-loop system can effectively suppress low frequency disturbance.
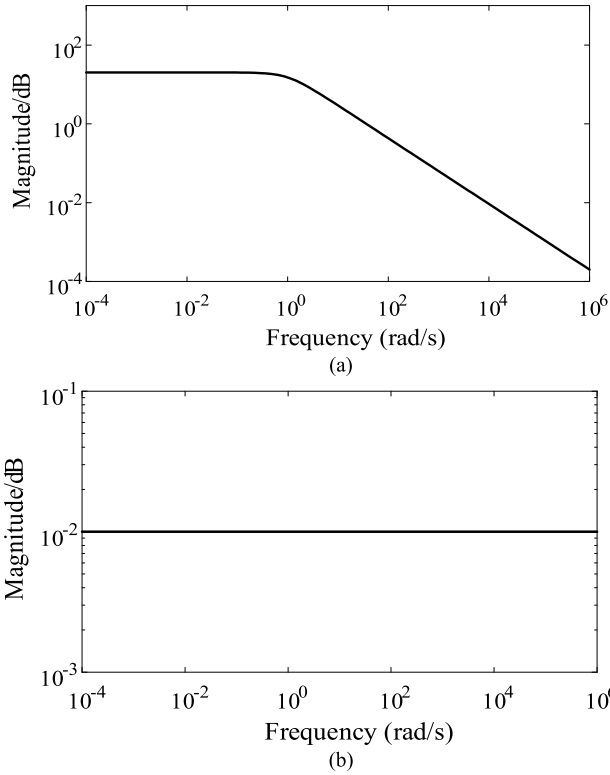
FIGURE 4. Amplitude-frequency response of weighting function.
(a) $W_P(s)$. (b) $W_u(s)$.

W_u is weighting function of the KS. The use of W_u can limit the size of the control amount and prevents the serious saturation phenomenon in the actual process, that is, the excessive control amount can cause damage to the actuator. W_u is used to describe norm bounds of parameter perturbation at low frequency ranges. Similar design principle is adopted according to the selection of weighting function in literatures [25]–[26]. W_p and W_u reflect the performance requirements of different frequency bands of the system. So they are selected as (24) according to the system parameters and the above design idea.

$$W_p = \frac{200}{s+1} , \quad W_u = 0.01 \tag{24}$$

In summary, the amplitude-frequency characteristic of each weighting function is shown in Fig. 4.

By substituting G into the robust control toolbox of MATLAB with *dkit* command [27]–[28], the μ robust controller of the dual LCL type IPT system can be calculated.

B. μ-SYNTHESIS: D-K ITERATION METHOD

In order to reflect the effect of the designed μ-controller, the structural singular value (μ) is introduced to determine the robustness under the control of parameters perturbation system, and a standard M-Δ structure is used for analysis as shown in Fig. 5. P (including the nominal object G_{mds}, W_p and W_u) represents a generalized object. Transfer function matrix $M \in R^{n*n}$ is obtained by the lower LFT of P and K. Δ_p is set of
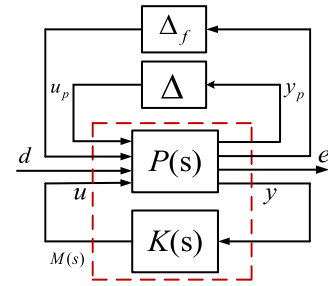

FIGURE 5. Standard M-Δ diagram of with *K*.

uncertainty matrix blocks. The first uncertain block Δ of the structural matrix is the uncertainty of the dual LCL-type IPT system modelling and is assumed $||\Delta||_\infty < 1(\Delta(s) \in RH_{\infty t})$. The second block Δ_f is virtual uncertain blocks that represents the performance requirement of the system.

$$\Delta_P = \left\{ \begin{bmatrix} \Delta & 0 \\ 0 & \Delta_f \end{bmatrix} : \Delta \in C^{9*9}, \Delta_f \in C^{1*2} \right\} \tag{25}$$

The robust performance comprehensive analysis can be attributed to finding a stable controller that keeps the closed-loop system stable with all possible uncertainties existing in the system possibly. The μ synthesis problem can be attributed to satisfying the following conditions.

$$\left\| \mu_{\Delta_p} [F_L(P, K)] \right\|_\infty < 1 \tag{26}$$

For optimal condition

$$\min_{K \text{ stabilize} P} \left\| \mu_{\Delta_p} [F_L(P, K)] \right\|_\infty \tag{27}$$

$\mu_{\Delta_p}[F_L(P, K)]$ can be calculated by selecting a scale matrix D, so the μ-synthesis problem is converted into

$$\inf_{K \text{ stablize} P} \sup_{\omega \in R} \inf_{D \in D} \mu \left[DF_L(P(j\omega), K(j\omega))D^{-1} \right] \tag{28}$$

For a given $\omega \in R$ (real number set), the matrix D that minimizes the maximum singular value of the above equation may be different. The problem can be described as

$$\inf_{K \text{ stabilize} P} \inf_{D \in D} \left\| DF_L(P, K)D^{-1} \right\|_\infty \tag{29}$$

For the above problem, *D-K* iterative algorithm design flowchart is shown as Fig. 6. The specific design process is as follows:

(1) Selecting the initial scaling matrix $D(s) = I$ (I is the identity matrix);

Defining a diagonal transfer function matrix $\widehat{D}$:

$$\widehat{D} = \begin{cases} D = diag[D_1, ..., D_s, d_1 I_{m1}, ..., d_f I_{mf}] : D_i \in C^{r_i * r_i} \\ D_i = D_i^* > 0, \ d_j > 0 \end{cases} \tag{30}$$

(2) For a given stable real rational minimum phase $D(s)$, solve the H_∞ optimal design problem and get the controller $K(s)$;
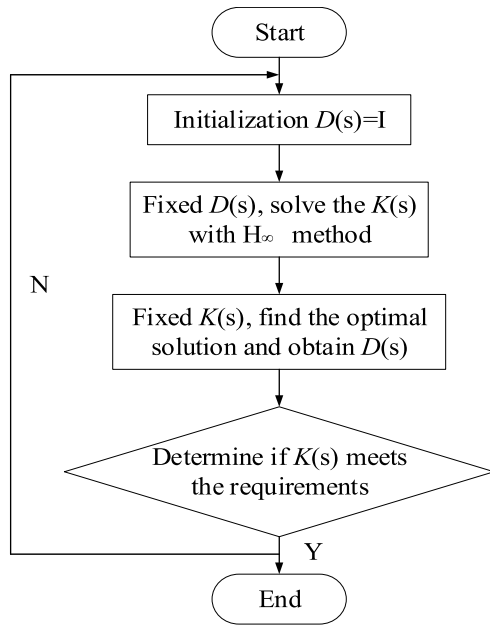
$$\inf_{K \text{ stabilize} P} \left\| DF_L(P, K)D^{-1} \right\| \tag{31}$$

FIGURE 6. Design flowchart of *D-K* iterative algorithm.

FIGURE 7. Frequency response of high-order and reduced-order controllers.

(3) For given $K_{(s)}$, solve optimal question and obtain the scale matrix $D_{(s)}$;

$$\inf_{D \in D} \mu[DF_{\mathrm{L}}(P, K)D^{-1}] \qquad (32)$$

Select a finite number of frequency points within the specified frequency range, corresponding to constant matrix D_{ω}, which may have different values at different frequencies, solve the optimization problem at each frequency point:

$$\min_{D \in D} \left\| D_{\omega} F_{\mathrm{L}}(P(j\omega), K(j\omega))D_{\omega}^{-1} \right\|_{\infty} \qquad (33)$$

Thus, it will get stable real rational minimum phase transfer function matrix $D(s)$ by fitting the curve.

(4) Repeat the above process until the iteration value meets the performance requirements of the design.

The iteration results are shown in Table 1. It can be seen from Table 1 that the μ value of the closed-loop system is decreasing and the robustness of the system is increasing according to the $D - K$ iterative algorithm described in the previous section. By the end of the last iteration, the iterative μ value gets 0.959, which reaches the preset performance of the closed-loop system.

TABLE 1. Iteration results.

Iteration	Control Order	Gamma Achieved	Peak mu-Value
1	4	1.334	1.274
2	22	1.111	1.106
3	24	0.961	0.959

C. CONTROL PERFORMANCE ANALYSIS

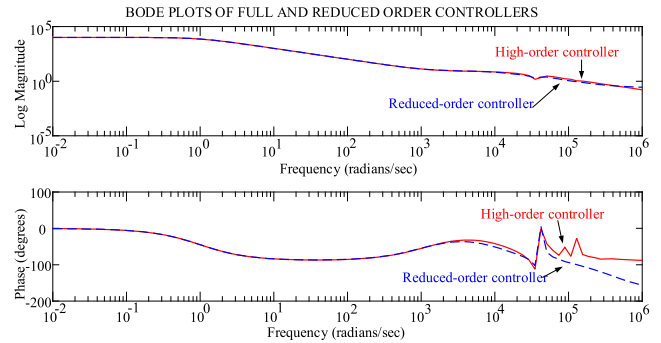In the design process, the μ-controller is a high-order controller due to the scalar scale matrix D. It is necessary to

perform the reduced-order processing by a certain method and ensure that the performance of the closed-loop system of the two controllers is almost the same. The verification can be performed by the frequency response of the nominal performance, robust stability, robust performance and sensitivity analysis of the reduced-order controller.

According to the controller reduction principle based on the *Hankel-norm* approximation method, the order of the reduced order controller is 10th order (in Appendix C). As shown in Fig. 7, the frequency response of the high-order and reduced-order controllers is almost identical and the frequency can be close to 10^5 rad/s.

1) NOMINAL PERFORMANCE ANALYSIS
When analyzing the nominal performance under μ control, the uncertainties affecting the accuracy of the model are not taken into account. For nominal plant G_{mds}, nominal performance can be represented by transfer function matrix T_{dz} from external disturbance d to tuned output $z = [e_{\mathrm{p}}, e_{\mathrm{u}}]^{\mathrm{T}}$ according to Fig. 3. That is:

$$||T_{\mathrm{dz}}||_{\infty} = \left\| \begin{bmatrix} W_{\mathrm{p}}(I + G_{\mathrm{mds}}K)^{-1} \\ W_{\mathrm{u}}K(I + G_{\mathrm{mds}}K)^{-1} \end{bmatrix} \right\|_{\infty} < 1 \qquad (34)$$

The nominal performance frequency response of the closed-loop system is shown in Fig. 8, it can be seen that the amplitude-frequency response of the closed-loop transfer function is less than 1 at any value in the frequency range $[10^{-2}, 10^6]$ under the μ-synthesis control from Fig. 8. This shows that the μ-synthesis control system is not only internally stable, but also achieves the preset nominal requirement.

After obtaining the μ-controller, μ analysis method is used to test the RSRP of closed-loop system to prove the expected performance requirements of the closed-loop system under various uncertainties and external disturbance factors.

2) ROBUST STABILITY ANALYSIS
The frequency response of the robust stability analysis is shown in Fig. 9. The horizontal axis is the frequency (rad/s) and the vertical axis is the μ value. The closed loop system with μ-controller has robust stability if and only if the condition of $\sup_{\omega \in R} \mu_{\Delta}(\mathrm{M}) < 1$ is satisfied. It can be seen that
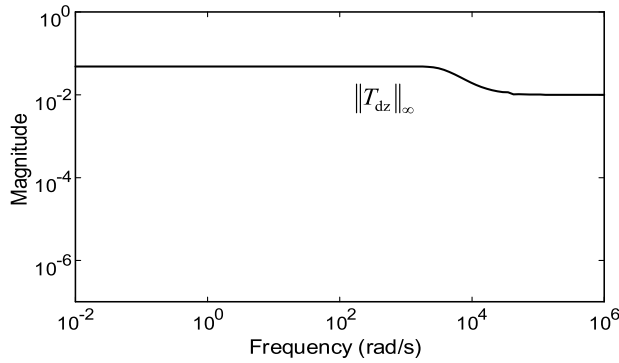
FIGURE 8. Nominal performance frequency response of closed-loop system.
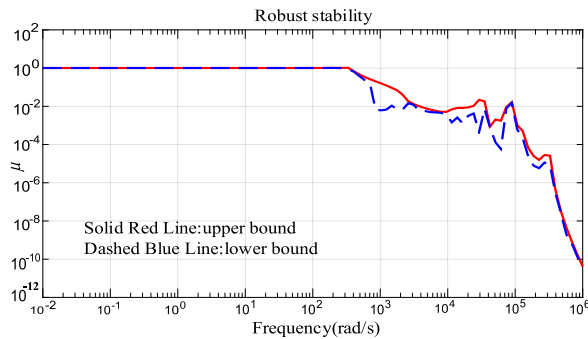

FIGURE 9. Frequency response of robust stability.

the upper and lower bounds of $\mu_\Delta(M)$ are both less than 1. It meets the design requirement.

3) ROBUST PERFORMANCE ANALYSIS

Closed-loop system not only need to satisfy robust stability, but also have robust performance under the influence of structural uncertainty. Fig. 10 shows the $\mu_\Delta[F_L(P, K)]$ frequency response of the robust performance of the closed-loop system. The horizontal axis is the frequency and the vertical axis is $\mu_\Delta[F_L(P, K)]$ value. It can be seen from the figure that the value of $\mu_\Delta[F_L(P, K)]$ is always less than 1 over the entire frequency ranges. It satisfies the robust performance. The largest μ value on the waveforms in the figure is 0.528. So the perturbation range allowed by the closed-loop system is $||\Delta|| \leq 0.528^{-1}$.
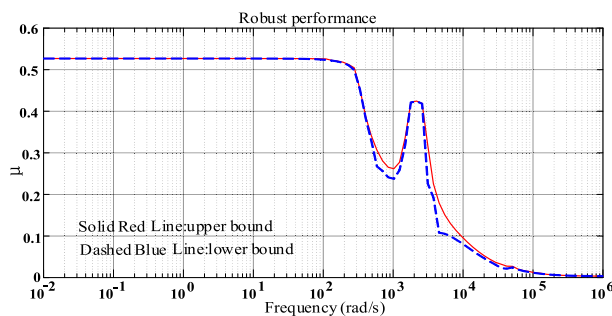
FIGURE 10. Frequency response of robust performance.

4) SENSITIVITY ANALYSIS

The sensitivity of closed-loop system is an important index to determine the error of system controller. Under the influence of various uncertainties and external disturbance, the gain of S of the system directly reflects the ability of the closed-loop system to suppress disturbances: the smaller the gain of the mixed sensitivity function, the stronger the anti-interference ability of the closed-loop system, and the smaller the control error of the system output under the influence of external disturbance.

It can be seen from equation (28) that the condition of μ-synthesis design can ensure the performance requirement of the closed-loop system. That is

$$\left\| \begin{bmatrix} W_p(I+GK)^{-1} \\ W_uK(I+GK)^{-1} \end{bmatrix} \right\|_\infty = \left\| \begin{bmatrix} W_pS \\ W_uKS \end{bmatrix} \right\|_\infty < 1 \quad (35)$$

In order to effectively suppress the influence of external disturbances on closed-loop perturbed system, the mixed sensitivity function according to formula (36) should satisfy the following constraint:

$$\|W_pS\|_\infty < 1 \quad (36)$$

This may be checked by computing the sensitivity function of the closed-loop system and comparing it with the inverse of the performance weighting function $(1/W_p)$. Sensitivity function with K is shown as Fig. 11.

As can be seen from Fig. 11, the amplitude-frequency response of the output sensitivity function is always below frequency response of the inverse performance weighting function under the μ control. In addition, the sensitivity function gain is always less than 1, which shows that the output error of the closed-loop system can be well suppressed when both bounded perturbation and external disturbance exist. Therefore, the closed-loop system with μ-controller has good anti-interference ability.

FIGURE 11. Sensitivity function with *K*.

D. ROBUST ANALYSIS OF CLOSED-LOOP PERTURBATION SYSTEM

For more intuitively describing the dynamic performance and stability of the closed-loop perturbation system, the time domain can be used. By setting the reference input and

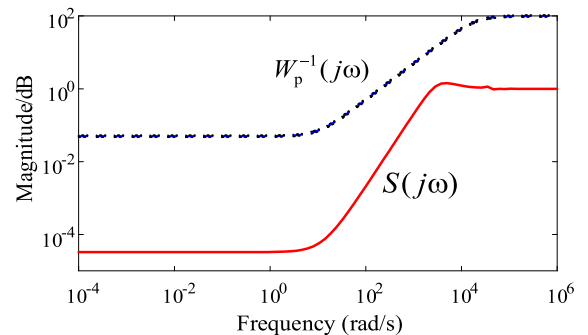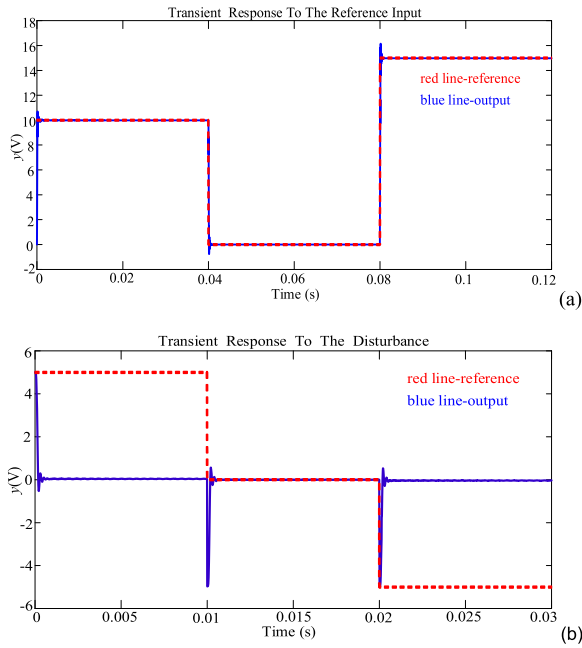**FIGURE 12.** Transient response of closed loop (a) Reference input change, (b) Disturbance change.

disturbance input, the motion equation of the closed-loop perturbation system is solved in the time domain to obtain the response curve of the system in the time domain. The transient response of the system at the reference input and the disturbance input are shown in Fig. 12(a) and Fig. 12(b) respectively. It can be seen from the figures that the designed controller can achieve better tracking and anti-interference effects, which proves the effectiveness of μ control.

V. SIMULATION AND EXPERIMENTS

In order to make robust design process more clearer and more useful for IPT system with dual LCL as well as other topologies, the design flowchart is given in Fig. 13.

Considering the requirements of the robust controller of the dual LCL closed-loop system, the selected circuit parameters are shown in Table 2 according to the circuit topology.

TABLE 2. Circuit parameters table.

Parameters	Values
Input voltage source E_{dc}/V	60
Invert frequency f/kHz	20
Primary coil inductance L_{p1}/μH	111.12
Equivalent resistance R_{Lp}/Ω	0.106
Primary LCL inductance L_{p2}/μH	111.12
Primary resonant capacitance C_p/μF	0.52
Secondary coil inductance L_{s1}/μH	111.36
Equivalent resistance R_{Ls}/Ω	0.102
Secondary LCL inductance L_{s2}/μH	111.36
Secondary resonant capacitance C_s/μF	0.52
Mutual inductance M/μH	49.71
Filter capacitance C_f/μF	47
Load R_L/Ω	20
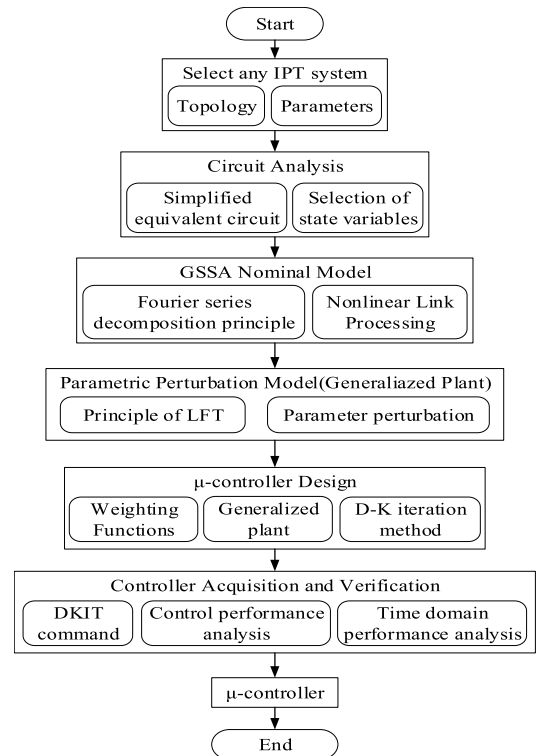
FIGURE 13. Design flowchart of μ control.

A. SIMULATION ANALYSIS

In order to verify the tracking effect of the output voltage under the μ control during the system start-up process, the simulation time of the system is set to be 0.08s during the simulation, and the reference output voltage of the system is set to be 10V at 0s and 15V at 0.04s respectively. The output voltage tracking characteristics of the system are shown in Fig. 14(a) under the action of the controller. The setting time is 1.3ms and the overshoot is almost 0% in the start-up process. 2.1% overshoot and 4.5ms setting time can be found during the switching. It has good tracking characteristic of the system.

According to the theoretical analysis, the closed-loop feedback system has the characteristic of suppressing external disturbance. The initial input voltage is 60V at 0s and disturbance of 20V is added after 0.04s in the simulation process. The setting time of the waveforms shown in Fig. 14 (b) is shorter and the overshoot is 6.7%, so the anti-interference characteristic meets the design requirements.

An important feature of the closed-loop feedback system based on μ-controller is to suppress the perturbation of system parameters. Fig. 14(c) analyses the closed-loop system with load perturbation. When the load changes from 20 Ω to 10 Ω, the system can also quickly track the given reference voltage with 5% overshoot after 3 ms. The response waveform of the mutual inductance change is shown in Fig. 14(d). It can be seen that there is setting time of 7ms and overshoot of 10% with changing. Therefore, the control system has better suppression of parameter perturbation characteristic.
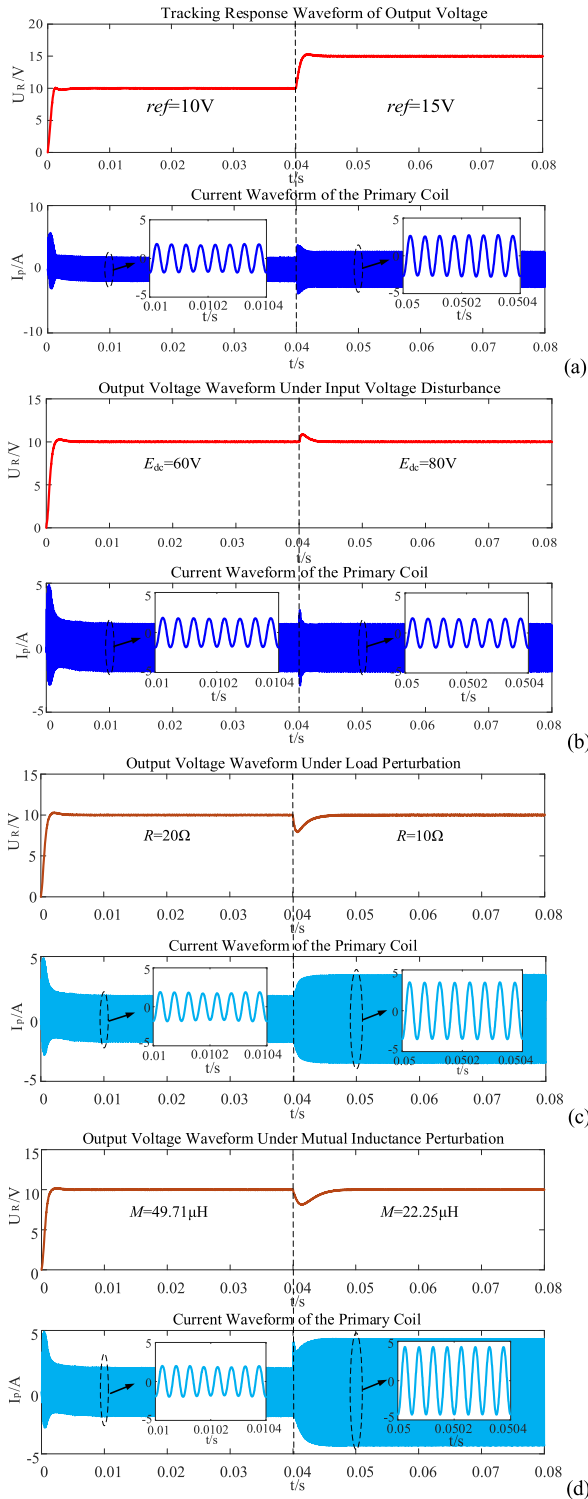
FIGURE 14. Output voltage and primary coil current waveforms. (a) Tracking response waveform, (b) Input voltage interference, (c) Load perturbation, (d) Mutual inductance perturbation.

In order to further verify the anti-interference characteristic of the system, the simulation diagram of output voltage waveform of the system under white noise disturbance is given. The white noise disturbance of the finite bandwidth is superimposed on the output voltage signal during the simulation.
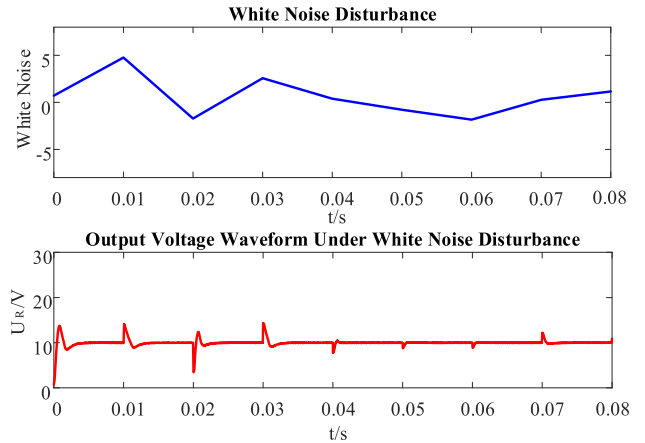
FIGURE 15. Output voltage waveform under white noise disturbance.

The white noise disturbance of the limited bandwidth can be directly generated in the simulink module "Band-limited-white-noise". The "Noise power" is set to 0.04. "Sample time" is 0.01 and "Seed" is 23341.

Fig. 15 shows white noise disturbance waveform and output voltage waveform. Under the action of white noise disturbance, the output voltage of the system fluctuates to a certain extent, but it can quickly track the reference voltage value to achieve stable output. Under the same control law, the magnitude of the fluctuation and recovery time are related to the size of the white noise interference. The larger the disturbance, the larger the fluctuation and the longer the recovery time.

B. EXPERIMENTAL RESULTS

In order to further verify that the dual LCL closed-loop control system based on μ-controller can maintain robust stability and robust performance under parameters perturbation and external disturbance, the parameters used in the experiment are consistent with the simulation parameters. The experimental schematic diagram is shown in Fig. 16, and the experimental platform for establishing the system is shown in Fig. 17. It adds Buck circuit as the input based on the original structure in the experiment. The load output voltage U_o is measured and sampled by the sampling circuit of the Hall sensor module (CHV-25P), and the voltage is received through the ESP8266WIFI module and information
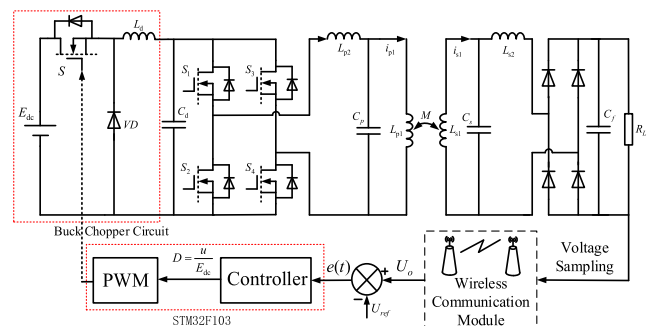
FIGURE 16. Schematic diagram.
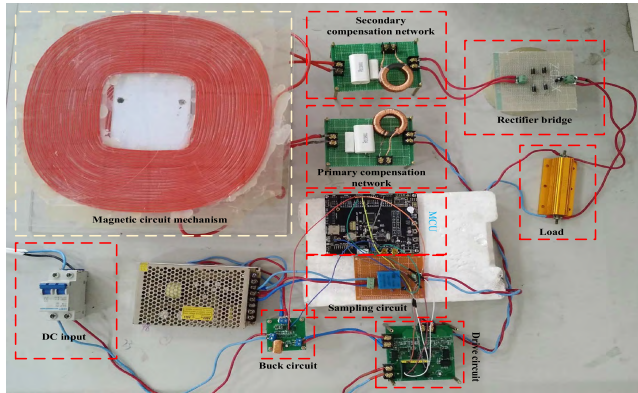
FIGURE 17. Experimental platform.

FIGURE 18. Experimental steady state waveforms of load output voltage U_o, inverter output voltage u_{in} and primary coil current i_{Lp}.

is sent to the controller. The *Hankel-norm* approximation method is used to reduce the order of the controller to obtain a 10th order controller. In order to obtain better control effect, the robust controller performs discretization processing and uses STM32F103 for controller operation and PWM output, which is converted into the driving signal of the Buck circuit and provides drive signal for the inverter. The Buck circuit chopping frequency is 50 kHz, the input voltage is 60 V, the filter inductance L_d is 1mH, and the output capacitance C_d is 100 uF.

In the experiment, the buck output voltage is equal to the output of the μ-controller. Under pulse width modulation, the turn-on ratio of the switching transistor of the buck circuit in one cycle is

$$D = \frac{u}{E_{dc}} \quad (37)$$

Through the above analysis, the performance of the low-order continuous controller is almost similar to that of the original high-order μ-controller. The low-order continuous μ-controller obtained in the previous section IV needs to be discretized in order to better handle and ensure real-time regulation of the system in STM32F103. The discretization method and the sample time step size affect the accuracy of the discrete controller; the accuracy of the discrete controller can also be reflected by the output response. In this paper, the equivalent digital controller is obtained based on Tustin Transformation's discretization method. This method can match well in frequency domain between continuous time and discrete time models. In the process of discretization, the sampling period of $T_s = 1$ us is short enough to ensure certain calculation accuracy. The discrete controller is

$$u(k) = \sum_{i=1}^{10} a_i \cdot u(k-i) + \sum_{j=0}^{10} b_j e(k-j) \quad (38)$$

$u(k)$ represents the control signal corresponding to the input voltage, and $e(k)$ represents the difference between the reference voltage and the output voltage. The signal a_i, b_j
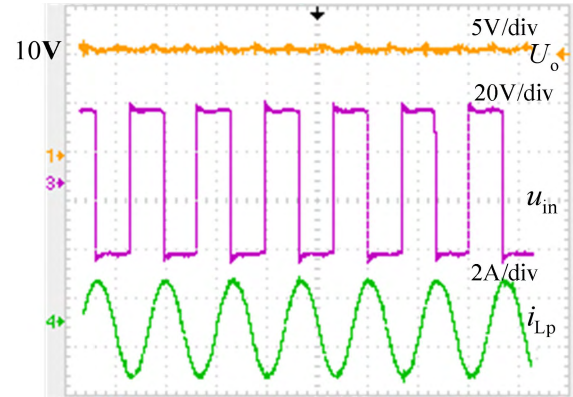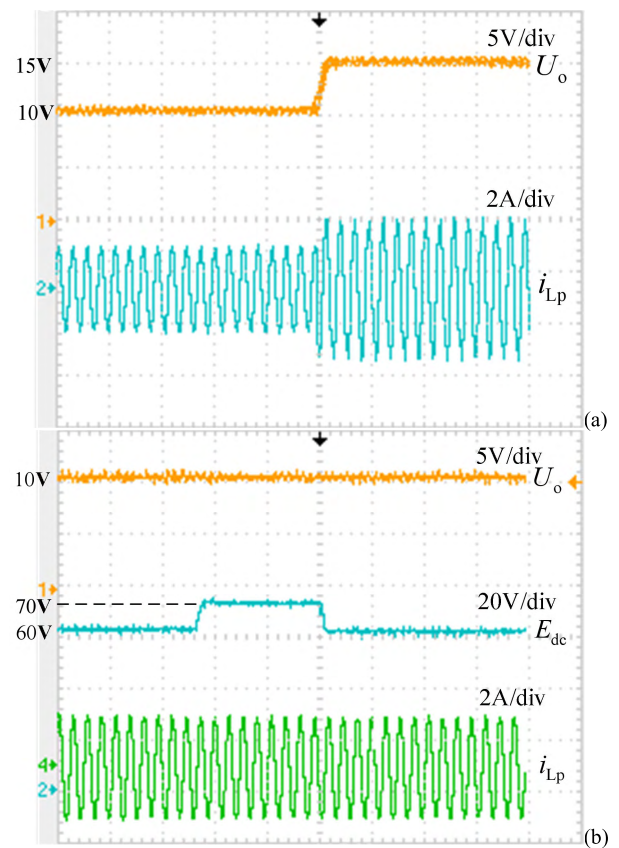
FIGURE 19. Experimental waveforms of load output voltage U_o, inverter output voltage u_{in} and primary coil current i_{Lp}. (a) Tracking response, (b) Input voltage disturbance.

are respectively.

$[a_1, \ldots a_{10}]$
$= [-0.8362, -0.2315, 0.8815, -0.3187, -0.1415,$
$\quad -0.7934, 0.6637, 0.06339, -0.6294, 0.3385] \quad (39)$

$[b_0, \ldots b_{10}]$
$= [3.241, -0.6377, -1.231, 3.42, 0.7312, -0.1805,$
$\quad -3.114, 1.1, 1.144, -2.934, 3.005e-31] \quad (40)$
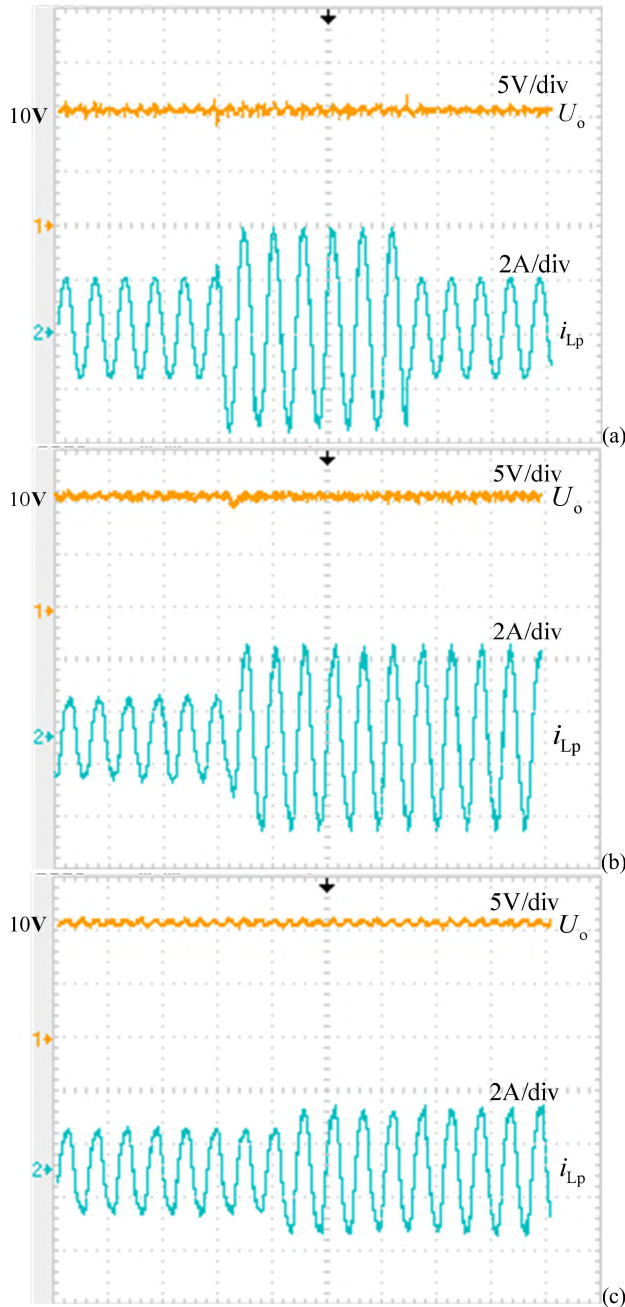
FIGURE 20. Experimental waveforms of load output voltage U_o and primary coil current i_{Lp}. (a) load perturbation, (b) Mutual inductance perturbation(49.71 μ H→ 22.25μH), (c) Mutual inductance and load changes(20Ω, 49.71μ H→ 10Ω,34.80μ H).

In order to verify the tracking output effect of the system at the start-up time, the output voltage is set to be 10 V and the output voltage U_0 and the waveform of the primary current i_{Lp} in the steady state is tested as shown in Fig. 18. The system can reach steady state. The output voltage waveform of primary inverter and the current waveform of primary coil have a phase difference of 90° after the steady state, which is in consistent with the characteristics of the LCL network

under the action of the controller. The primary coil current is a sinusoidal waveform with a lower distortion.

In order to verify the tracking effect of the controller, the system output is set from 10 V to 15 V. It can be seen from the Fig. 19(a) that the response time is 11ms, the response waveform has almost no overshoot and good tracking reference output voltage.

In the dual LCL type IPT system, the input voltage is disturbed by fluctuation of the power grid. The initial input voltage is set to 60V and input voltage interference of 10V is added at some point. The system response waveform is shown in Fig. 19(b). It can be seen that i_{Lp} remains unchanged. The output voltage reaches a steady state after a short dynamic process and achieves anti-interference effect.

In order to verify the robust control effect of the control method under the perturbation of load and mutual inductance, the expected output voltage is set to be 10V with load changing from 20 Ω to 10Ω in the first switching and changing from 10 Ω to 20 Ω in the second switching. The experimental waveform of the load perturbation is shown in Fig. 20(a). During the load variation process, the output voltage enters the steady state after the less adjustment process. There is the overshoot of 22% and it costs about 20ms in the process of load switching. The current waveform of primary coil still has good sinusoidal characteristics. The experimental waveforms of the the mutual inductance perturbation are shown in Fig. 20(b). It can be seen from the figure that it has smaller overshoot of 20%, setting time of 25ms and the output voltage quickly reaches the desired set value under the action of the μ-controller when the system receives the perturbation of the mutual inductance parameter. Fig. 20(c) is output waveforms with two parameters changing in the system. When the parameters change, the output voltage is overshoot of 18% and can reach the set value quickly. The designed controller has better control effect. It can be seen that the closed-loop system has better robustness and the effect of suppressing parameters perturbation under μ control.

VI. CONCLUSION

Aμ-synthesis robust control for the dual LCL IPT system of the closed-loop system with the uncertainty of load and mutual inductance parameters is proposed and developed in this paper. The linearized nominal frequency domain model and uncertainty model of double LCL topology are established based on the GSSA method and LFT principle. A μ-controller is designed by using *D-K* iterative method, and the control performance and transient performance of the system are both analyzed in this work. Experimental results show that the closed-loop system can quickly and accurately track the reference voltage, effectively suppress the influence of external disturbance and parameters perturbation and obtain output robustness. μ-synthesis control is characterized by the ability to obtain RSRP of system

$$G_k = \frac{\begin{matrix} 2.508e-5s^{10} + 1.12e4s^9 + 1.63e8s^8 + 4.536e14s^7 + 4.6e18s^6 + \\ 6.06e24s^5 + 3.8e28s^4 + 2.86e34s^3 + 1.04e38s^2 + 3.038e43s + 7.237e46 \end{matrix}}{\begin{matrix} s^{10} + 1.9e4s^9 + 4.1e10s^8 + 6.04e14s^7 + 5.45e20s^6 + 5.919e24s^5 + \\ 2.6e30s^4 + 2.04e34s^3 + 2.77e39s^2 + 1.64e43s + 1.64e40 \end{matrix}}$$

with respect to structural perturbations. At the same time, it can avoid unnecessary conservative design. The control method developed in this paper can also be applied to such uncertain systems in view of the complex dynamic behavior of IPT systems and has good application value in IPT system.

APPENDIX A

$$A = \begin{bmatrix}
0 & \omega & \frac{-1}{L_{p2}} & 0 & 0 & 0 & 0 & 0 & 0 & 0 & 0 & 0 & 0; \\
-\omega & 0 & 0 & \frac{-1}{L_{p2}} & 0 & 0 & 0 & 0 & 0 & 0 & 0 & 0 & 0; \\
\frac{1}{C_p} & 0 & 0 & \omega & \frac{1}{C_p} & 0 & 0 & 0 & 0 & 0 & 0 & 0 & 0; \\
0 & \frac{1}{C_p} & -\omega & 0 & 0 & \frac{1}{C_p} & 0 & 0 & 0 & 0 & 0 & 0 & 0; \\
0 & 0 & \frac{-L_{s1}}{det} & 0 & \frac{-L_{s1}R_{p1}}{det} & \omega & \frac{MR_{s1}}{det} & 0 & \frac{M}{det} & 0 & 0 & 0 & 0; \\
0 & 0 & 0 & \frac{-L_{s1}}{det} & -\omega & \frac{-L_{s1}R_{p1}}{det} & 0 & \frac{MR_{s1}}{det} & 0 & \frac{M}{det} & 0 & 0 & 0; \\
0 & 0 & \frac{M}{det} & 0 & \frac{-MR_{p1}}{det} & 0 & \frac{-L_{p1}R_{s1}}{det} & \omega & \frac{-L_{p1}}{det} & 0 & 0 & 0 & 0; \\
0 & 0 & 0 & \frac{M}{det} & 0 & \frac{-MR_{p1}}{det} & -\omega & \frac{-L_{p1}R_{s1}}{det} & 0 & \frac{-L_{p1}}{det} & 0 & 0 & 0; \\
0 & 0 & 0 & 0 & 0 & 0 & \frac{1}{C_s} & 0 & 0 & \omega & \frac{-1}{C_s} & 0 & 0; \\
0 & 0 & 0 & 0 & 0 & 0 & 0 & \frac{1}{C_s} & -\omega & 0 & 0 & \frac{-1}{C_s} & 0; \\
0 & 0 & 0 & 0 & 0 & 0 & 0 & 0 & \frac{1}{L_{s2}} & 0 & 0 & \omega & \frac{-2}{\pi L_{s2}}; \\
0 & 0 & 0 & 0 & 0 & 0 & 0 & 0 & 0 & \frac{1}{L_{s2}} & -\omega & 0 & 0; \\
0 & 0 & 0 & 0 & 0 & 0 & 0 & 0 & 0 & 0 & \frac{4}{\pi C_f} & 0 & \frac{-1}{C_f R_L}
\end{bmatrix}$$

$$B = \begin{bmatrix} 0, & \frac{-2}{\pi L_{p2}}, & 0, & 0, & 0, & 0, & 0, & 0, & 0, & 0, & 0, & 0, & 0 \end{bmatrix}^T;$$

$$C = [0\,0\,0\,0\,0\,0\,0\,0\,0\,0\,0\,0 - 1];$$

$$D = 0.$$

APPENDIX B

$$\begin{bmatrix} B_1 \\ B_2 \end{bmatrix} = \begin{bmatrix} 0\,0\,0\,0\,0\,0\,0\,0\,0\,0\,0\,0\,\frac{1}{R_0} \\ 0\,\frac{-2}{\pi L_{p2}}\,0\,0\,0\,0\,0\,0\,0\,0\,0\,0\,0 \end{bmatrix}^T;$$

$$A = \begin{bmatrix}
0 & \omega & \frac{-1}{L_{p2}} & 0 & 0 & 0 & 0 & 0 & 0 & 0 & 0 & 0 & 0; \\
-\omega & 0 & 0 & \frac{-1}{L_{p2}} & 0 & 0 & 0 & 0 & 0 & 0 & 0 & 0 & 0; \\
\frac{1}{C_p} & 0 & 0 & \omega & \frac{-1}{C_p} & 0 & 0 & 0 & 0 & 0 & 0 & 0 & 0; \\
0 & \frac{1}{C_p} & -\omega & 0 & 0 & \frac{1}{C_p} & 0 & 0 & 0 & 0 & 0 & 0 & 0; \\
0 & 0 & \frac{-L_{s1}}{det} & 0 & \frac{-L_{s1}R_{p1}}{det} & \omega & \frac{MR_{s1}}{det} & 0 & \frac{M}{det} & 0 & 0 & 0 & 0; \\
0 & 0 & 0 & \frac{-L_{s1}}{det} & -\omega & \frac{-L_{s1}R_{p1}}{det} & 0 & \frac{MR_{s1}}{det} & 0 & \frac{M}{det} & 0 & 0 & 0; \\
0 & 0 & \frac{M}{det} & 0 & \frac{-MR_{p1}}{det} & 0 & \frac{-L_{p1}R_{s1}}{det} & \omega & \frac{-L_{p1}}{det} & 0 & 0 & 0 & 0; \\
0 & 0 & 0 & \frac{M}{det} & 0 & \frac{-MR_{p1}}{det} & -\omega & \frac{-L_{p1}R_{s1}}{det} & 0 & \frac{-L_{p1}}{det} & 0 & 0 & 0; \\
0 & 0 & 0 & 0 & 0 & 0 & \frac{1}{C_s} & 0 & 0 & \omega & \frac{-1}{C_s} & 0 & 0; \\
0 & 0 & 0 & 0 & 0 & 0 & 0 & \frac{1}{C_s} & -\omega & 0 & 0 & \frac{-1}{C_s} & 0; \\
0 & 0 & 0 & 0 & 0 & 0 & 0 & 0 & \frac{1}{L_{s2}} & 0 & 0 & \omega & \frac{-2}{\pi L_{s2}}; \\
0 & 0 & 0 & 0 & 0 & 0 & 0 & 0 & 0 & \frac{1}{L_{s2}} & -\omega & 0 & 0; \\
0 & 0 & 0 & 0 & 0 & 0 & 0 & 0 & 0 & 0 & \frac{4}{\pi C_f} & 0 & \frac{-1}{C_f R_0}
\end{bmatrix};$$

$$\begin{bmatrix} C_1 \\ C_2 \end{bmatrix} = \begin{bmatrix} 0\,0\,0\,0\,0\,0\,0\,0\,0\,0\,0\,0\,\frac{1}{R_0} \\ 0\,0\,0\,0\,0\,0\,0\,0\,0\,0\,0\,0 - 1 \end{bmatrix};$$

$$\begin{bmatrix} D_{11} & D_{12} \\ D_{21} & D_{22} \end{bmatrix} = \begin{bmatrix} -p_R & 0 \\ 0 & 0 \end{bmatrix}.$$

APPENDIX C
See the equation shown at the top of this page.

REFERENCES

[1] M. McDonough, "Integration of inductively coupled power transfer and hybrid energy storage system: A multiport power electronics interface for battery-powered electric vehicles," *IEEE Trans. Power Electron.*, vol. 30, no. 11, pp. 6423–6433, Nov. 2015.

[2] M. Debbou and F. Colet, "Inductive wireless power transfer for electric vehicle dynamic charging," in *Proc. IEEE PELS Workshop Emerg. Technol., Wireless Power Transf.*, Oct. 2016, pp. 118–122.

[3] S. Zhou, C. Zhu, S. Cui, Z. Wang, S. Zhou, and C. C. Chan, "Dynamic wireless power transfer system for electric vehicles employing multiplexing LCC modules with individual transmitters," *IEEE Access*, vol. 6, pp. 62514–62527, Nov. 2018.

[4] J. H. Kim, B.-S. Lee, J.-H. Lee, S.-H. Lee, C.-B. Park, S.-M. Jung, S.-G. Lee, K.-P. Yi, and J. Baek, "Development of 1-MW inductive power transfer system for a high-speed train," *IEEE Trans. Ind. Electron.*, vol. 62, no. 10, pp. 6242–6250, Oct. 2015.

[5] X. Shu, W. Xiao, and B. Zhang, "Wireless power supply for small household appliances using energy model," *IEEE Access.*, vol. 6, pp. 69592–69602, Nov. 2018.

[6] H. Jiang, J. Zhang, D. Lan, K. K. Chao, S. Liou, H. Shahnasser, R. Fechter, and S. Hirose, "A low-frequency versatile wireless power transfer technology for biomedical implants," *IEEE Trans. Biomed. Circuits Syst.*, vol. 7, no. 4, pp. 526–535, Aug. 2013.

[7] N. Dobrostomat, G. Turcan, and M. Neag, "Wearable health monitors with transfer jet data communications and inductive power transfer," in *Proc. Int. Semicond. Conf. (CAS)*, Sinaia, Romania, Oct. 2014, pp. 259–262.

[8] Z. Huang, S.-C. Wong, and C. K. Tse, "Control design for optimizing efficiency in inductive power transfer systems," *IEEE Trans. Power Electron.*, vol. 33, no. 5, pp. 4523–4534, May 2017.

[9] Z. Lin, J. Wang, Z. Fang, M. Hu, C. Cai, and J. Zhang, "Accurate maximum power tracking of wireless power transfer system based on simulated annealing algorithm," *IEEE Access*, vol. 6, pp. 60881–60890, Nov. 2018.

[10] Y. Wang, Y. Yao, X. Liu, and D. Xu, "S/CLC compensation topology analysis and circular coil design for wireless power transfer," *IEEE Trans. Transport. Electrific.*, vol. 3, no. 2, pp. 496–507, Jun. 2017.

[11] R. Mai, Y. Chen, Y. Li, Y. Zhang, G. Cao, and Z. He, "Inductive power transfer for massive electric bicycles charging based on hybrid topology switching with a single inverter," *IEEE Trans. Power Electron.*, vol. 32, no. 8, pp. 5897–5906, Aug. 2017.

[12] J. L. Villa, J. Sallan, J. F. S. Osorio, and A. Llombart, "High-misalignment tolerant compensation topology for ICPT systems," *IEEE Trans. Ind. Electron.*, vol. 59, no. 2, pp. 945–951, Feb. 2012.

[13] S. Zhou and C. Mi, "Multi-paralleled LCC reactive power compensation networks and its tuning method for electric vehicle dynamic wireless charging," *IEEE Trans. Ind. Electron.*, vol. 63, no. 10, pp. 6546–6556, Jan. 2016.

[14] A. Namadmalan, "Self-oscillating tuning loops for series resonant inductive power transfer systems," *IEEE Trans. Power Electron.*, vol. 31, no. 10, pp. 7320–7327, Oct. 2016.

[15] H. Hao, G. A. Covic, and J. T. Boys, "An approximate dynamic model of LCL-T-based inductive power transfer power supplies," *IEEE Trans. Power Electron.*, vol. 29, no. 10, pp. 5554–5567, Oct. 2014.

[16] F. F. A. van der pijl, M. Castilla, and P. Bauer, "Adaptive sliding-mode control for a multiple-user inductive power transfer system without need for communication," *IEEE Trans. Power Electron.*, vol. 60, no. 1, pp. 271–279, Jan. 2013.

[17] Y. Li, H. Du, M. Yang, and Z. He, "Two-degree-of-freedom H$_\infty$ robust control optimization for IPT system with parameter perturbations," *IEEE Trans. Power Electron.*, vol. 33, no. 12, pp. 10954–10969, Dec. 2018.

[18] C. Xia, W. Wang, G. Chen, X. Wu, S. Zhou, and Y. Sun, "Robust control for the relay ICPT system under external disturbance and parametric uncertainty," *IEEE Trans. Control Syst. Technol.*, vol. 25, no. 6, pp. 2168–2175, Nov. 2017.

[19] X. Dai, C. Tang, and Y. Sun, "Investigating a H$_\infty$ control method considering frequency uncertainty for CLC type inductively coupled power transfer system," in *Proc. IEEE. ECCE*, Sep. 2011, pp. 2022–2027.

[20] Y.-L. Li, Y. Sun, and X. Dai, "μ-synthesis for frequency uncertainty of the ICPT system," *IEEE Trans. Ind. Electron.*, vol. 60, no. 1, pp. 291–300, Jan. 2013.

[21] C. Xia, W. Wang, S. Ren, X. Wu, and Y. Sun, "Robust control for inductively coupled power transfer systems with coil misalignment," *IEEE Trans. Power Electron.*, vol. 33, no. 9, pp. 8110–8122, Sep. 2018.

[22] C.-S. Wang, G. A. Covic, and O. H. Stielau, "Investigating an LCL load resonant inverter for inductive power transfer applications," *IEEE Trans. Power Electron.*, vol. 19, no. 4, pp. 995–1002, Jul. 2004.

[23] J. T. Boys, G. A. Covic, and A. W. Green, "Stability and control of inductively coupled power transfer systems," *IEE Proc.-Electr. Power Appl.*, vol. 147, no. 1, pp. 37–43, 2013.

[24] A. P. Hu, "Modeling a contactless power supply using GSSA method," in *Proc. IEEE Int. Conf. Ind. Technol.*, Feb. 2009, pp. 1–6.

[25] H. Oloomi and B. Shafai, "Weight selection in mixed sensitivity robust control for improving the sinusoidal tracking performance," in *Proc. IEEE CDC*, Dec. 2003, pp. 300–305.

[26] A. E. Mhankale, A. B. Paul, and G. B. Chavan, "Robust control analysis using μ-synthesis for nonlinear control system," in *Proc. Int. Conf. Smart Grids, Power Adv. Control Eng. (ICSPACE)*, Aug. 2017, pp. 155–163.

[27] D.-W. Gu, P. Petkov, and M. M. Konstantinov, *Robust Control Design With MATLAB*. Berlin, Germany: Springer-Verlag, 2013.

[28] P. Apkarian, J. P. Chretien, P. Gahinet, and J. M. Biannic, "μ-synthesis by D-K iterations with constant scaling," in *Proc. IEEE Amer. Control Conf.*, Jun. 2009, pp. 3192–3196.

[29] X. Jin, G. Yin, Y. Li, and J. Li, "Stabilizing vehicle lateral dynamics with considerations of state delay of AFS for electric vehicles via robust gain-scheduling control," *Asian J. Control*, vol. 18, no. 1, pp. 89–97, 2015.

[30] G. Yin, N. Chen, and P. Li, "Study on maneuverability and stability of four-wheel steering vehicle based on robust μ-synthesis Control," *Eng. Sci.*, vol. 7, no. 4, pp. 54–58, Apr. 2005.

[31] K. Zhou, J. C. Doyle, and K. Glover, *Robust and Optimal Control*. Beijing, China: National Defense Industry Press, 2001, pp. 134–137.

[32] D. S. Bernstein and W. M. Haddad, "LQG control with an H$_\infty$ performance bound: A riccati equation approach," *IEEE Trans. Autom. Control*, vol. 34, no. 3, pp. 293–305, Mar. 1992.

CHENYANG XIA was born in Jiangsu, China, in 1982. He received the B.S., M.S., and Ph.D. degrees in control theory and control engineering from Chongqing University, Chongqing, China, in 2006, 2008, and 2010, respectively. From 2018 to 2019, he was an Academic Visitor with The University of Auckland, New Zealand. He is currently an Associate Professor with the School of Electrical and Power Engineering, China University of Mining and Technology, Xuzhou, China. His current research interests include wireless power transfer technology, power electronics, intrinsic safety switch power supply, and intelligent control.
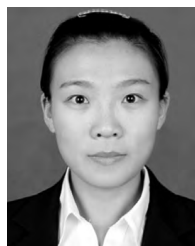
QIQI SUN was born in Jiangsu, China, in 1994. She received the B.S. degree in electrical engineering from the Qingdao University of Technology, Shandong, China, in 2016. She is currently pursuing the M.S. degree with the School of Electrical and Power Engineering, China University of Mining and Technology, Xuzhou, China. Her current research interests include power electronics and wireless power transfer technology.

XINYU LI was born in Ningxia, China, in 1996. He received the B.S. degree in electrical engineering from the China University of Mining and Technology, Xuzhou, China, in 2017, where he is currently pursuing the M.S. degree with the School of Electrical and Power Engineering. His current research interests include power electronics and wireless power transfer technology.

AIGUO PATRICK HU received the B.E. and M.E. degrees from Xian Jiaotong University, Xian, China, in 1985 and 1988, respectively, and the Ph.D. degree from The University of Auckland, Auckland, New Zealand, in 2001. He was a Lecturer and the Director of the China Italy Cooperative Technical Training Center, Xi'an, and the General Manager of a technical development company. Funded by Asian2000 Foundation, he was with the National University of Singapore for a semester as an Exchange Postdoctoral Research Fellow. He is currently with the Department of Electrical and Computer Engineering, The University of Auckland, and also the Head of Research of PowerbyProxi, Ltd. He holds 15 patents in wireless/contactless power transfer and microcomputer control technologies, published more than 200 peer-reviewed journal and conference papers, authored a monograph on wireless inductive power transfer technology, and contributed four book chapters.

• • •